VI International Conference on Computational Methods in Marine Engineering
MARINE 2015
F. Salvatore, R. Broglia and R. Muscari (Eds)

FINITE ELEMENT ANALYSIS OF HORIZONTAL AXIS WIND TURBINES PERFORMANCE

A. CALABRETTA[*], C. TESTA[*], L. GRECO[*] AND M. GENNARETTI[†]

[*] CNR-INSEAN Marine Technology Research Institute
Via di Vallerano 139, Rome, Italy
email: angelo.calabretta@uniroma3.it, www.insean.cnr.it

[†] Department of Engineering, Roma Tre University
Via della Vasca Navale 79, Rome, Italy
email: massimo.gennaretti@uniroma3.it, www.uniroma3.it

Key words: Wind turbines, Rotor Aeroelasticity, Finite Element Method

Abstract. This paper presents an aeroelastic formulation based on the Finite Element Method (FEM) to predict the performance of an isolated horizontal axis wind turbine. Hamilton's principle is applied to derive the equations of blade(s) aeroelasticity, based on a nonlinear beam model coupled with Beddoes-Leishman unsteady sectional aerodynamics. A devoted fifteen-degrees of freedom finite element, able to accurately model the kinematics and elastic behavior of rotating blades, is introduced and the spatial discretization of the aeroelastic equations is carried-out yielding a set of coupled nonlinear ordinary differential equations that are then solved by a time-marching algorithm. The proposed formulation may be enhanced to face the analysis of advanced blade shapes, including the presence of the tower, and represents the first step of an ongoing activity on wind energy based on a FEM approach. Due to similarities between wind turbine and helicopter rotor blades aeroelasticity, validation results firstly concern with the aeroelastic response of a helicopter rotor in hovering. Next, the performance of a wind turbine in terms of blade elastic response and delivered power are predicted and compared with available literature data.

1 INTRODUCTION

Wind energy provides an environmental friendly option for energy supply at a time when decreasing reserves of fossil fuel threatens the long-term sustainable development of economy. During the last decade, the size of wind turbine has increased dramatically from a rated power of 50 kW with rotors of 10–15 m diameter up to commercial 3–3.5MW turbines with rotors of 80–90 m diameters. More flexible and lower stiffness rotor blades lead to a stronger coupling between aerodynamics and structural dynamics; hence the aeroelasticity has become one of the most critical issues during the design process of modern wind turbines. The target of the research on aeroelasticity is to satisfy the requirements of the increasing size of wind turbine assuring at the same time, more efficient devices. To this aim, the availability of fast and reliable numerical prediction tools is mandatory for multidisciplinary optimization applications during the pre-design stage, when many engineering choices have to be validated.

These considerations have inspired the present work that proposes an aeroelastic formulation based on a Finite Element Method (FEM) for performance and stability prediction of isolated horizontal axis wind turbines. The formulation is general, in that it might be extended to configurations including the presence of the tower and floating structures for off-shore applications; it represents the starting point of an ongoing research activity on wind energy aimed at meeting the growing demand to better predict the delivered power of horizontal-axis wind turbines. Since wind turbines and helicopter rotors share similar aeroelastic problems affecting overall performance, vibration, loads, and stability [1], both structural and aerodynamic models come from those developed in [2], [3] and successfully applied to the study of rotorcraft aeroelasticity. This fact makes the present formulation not a novelty in the framework of wind turbine aeroelasticity; however, following [1], the level of accuracy in the physical description of the fluid-structure interaction makes the proposed approach among those having a leading position in wind turbine aeroelastic simulations.

Specifically, the theoretical modelling herein presented is applicable to turbine with non-uniform rotor blades, described as long, straight, slender, homogeneous isotropic beams undergoing axial, lag, flap and torsion displacements. The theory is intended for moderate displacements, accurate to second order and based on the hypothesis that squares of bending slopes, twist, thickness-radius and chord-radius ratios are small with respect to unity. The analysis is developed for an isolated turbine rotor having blades with pretwist, precone, and chord-wise offsets of the center of mass, aerodynamic center, and tension center from the elastic axis; structural dissimilarity among rotor blades are neglected whereas advanced tip shapes, such as swept-tip or tapered-tip, are not modelled. Blade aerodynamics is simulated by the unsteady sectional Beddoes-Leishman (B-L) state-space formulation which includes effects of nonlinear phenomena, such as static and dynamic stall, to yield a more realistic description of the aerodynamic environment. Wake inflow effects are modelled either by the simple momentum theory approach, or by a more advanced description obtained through an unsteady, three-dimensional, free-wake panel method [4, 5]. Aeroelastic blade equations are firstly obtained in weak-form through the application of Hamilton's principle; the resulting nonlinear partial-integral equations of motions are then reduced to a set of nonlinear ordinary differential equations by the spatial FEM-based discretization [6], then solved through a Crank-Nicolson time-marching scheme. Due to the similarities between helicopter and wind-turbine rotor blades, validation results with respect to literature data are firstly presented by studying the behaviour of a two-bladed helicopter main rotor in hovering in terms of steady-state aeroelastic blade-tip displacements and blade loads. Next, blade response and delivered power of a horizontal-axis wind turbine operating in an homogeneous onset-flow are predicted; the turbine configuration is that studied in the past by some of the authors through a well-assessed and validated aeroelastic modal approach based on the same structural and aerodynamic blade models used here [7]. Results from the FEM formulation have to be intended as preliminary.

2 AEROELASTIC MODELLING

In the following, the main aspects of the aeroelastic blade model are briefly discussed; more details are given in [2] and [3]. Firstly, the equations of blade motion are derived by

invoking Hamilton's principle without the presence of nonconservative aerodynamic loads, and the kinematics features of the finite elements are described. Then, the aerodynamic B-L model is presented and the generalized aerodynamic nodal forces are obtained.

2.1 Blade Dynamics

A nonlinear elastic blade model [2, 3] is used in present analysis. The blade is assumed to be an elastic beam undergoing flap and lag bending, elastic twist and axial deformation. Governing equation of motion are derived from the generalized Hamilton's principle applicable to non-conservative systems

$$\delta\Pi = \int_{\Psi_1}^{\Psi_2} (\delta U - \delta T - \delta W)\, d\Psi = 0 \tag{1}$$

with $\Psi_{1,2}$ defining the azimuth angles between which motion is analyzed whereas δU , δT and δW represent the virtual strain energy, kinetic energy and work done by external forces, respectively, written as sum of contributions from each rotor blade. A detailed derivation of virtual energies δU and δT may be found in [2]. Equations of motions are based on the work of Hodges and Dowell [2] and include second-order geometric nonlinear terms accounting for moderate deflections in flap, lag, axial and torsion equations. In the context of a finite element approach (see, for instance, [6]) each blade is discretized into a number of beam elements, having fifteen degrees of freedom (DOFs) distributed over five element nodes (2 boundary nodes and 3 interior nodes). There are six degrees of freedom at each element boundary node, corresponding to u (axial displacement), v (lag deflection), v' (lag bending-slope), w (flap deflection), w' (flap bending-slope), ϕ (twist) (see Figs. 1 and 2 for details).

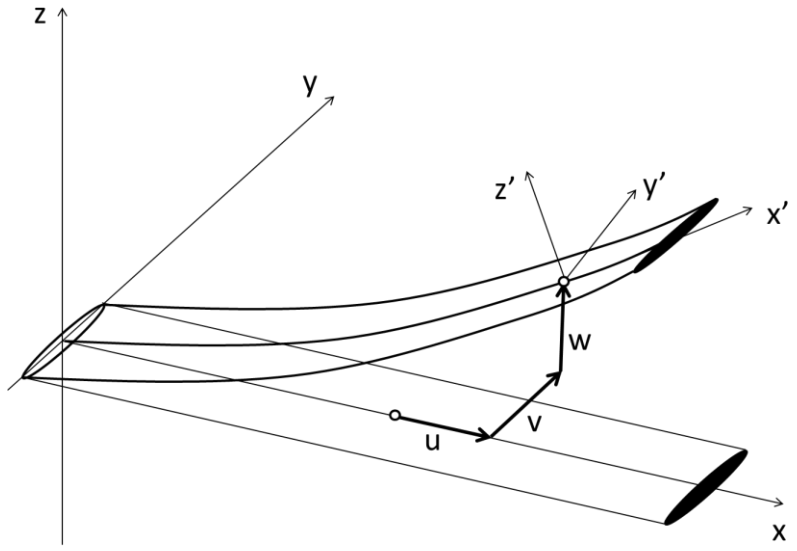

Figure 1: Blade elastic displacements and undeformed/deformed frames of reference

Moreover, there are two internal nodes for elastic axial deflection and one internal node for the elastic twist (see Fig. 2). These DOFs correspond to cubic variations of the axial and flap-lag bending deflections and quadratic variation of the elastic torsion. Between elements, continuity of displacements and slope for flap-lag deflections, as well as continuity of displacements for elastic twist and axial deflections, are assured. This kind of element provides physically consistent linear variations of bending and torsional moments, and quadratic variation of axial force within each element. Geometric and structural properties are assumed to be constant within each element, with the exception of blade pre-twist. The shape functions used for FEM discretization are Hermite polynomials for lag and flap bending and Lagrange polynomials for axial and torsional deflections. For the *i-th* beam element, the elastic displacements may expressed as

$$\mathbf{u}_i(\xi,t) = \mathbf{H}(\xi)\,\mathbf{q}_i(t) \tag{2}$$

where $\mathbf{H}$ is the shape function matrix and $\mathbf{q}_i$ is the vector of the elemental DOFs defined accordingly to the nodal topology shown in Fig. 2.

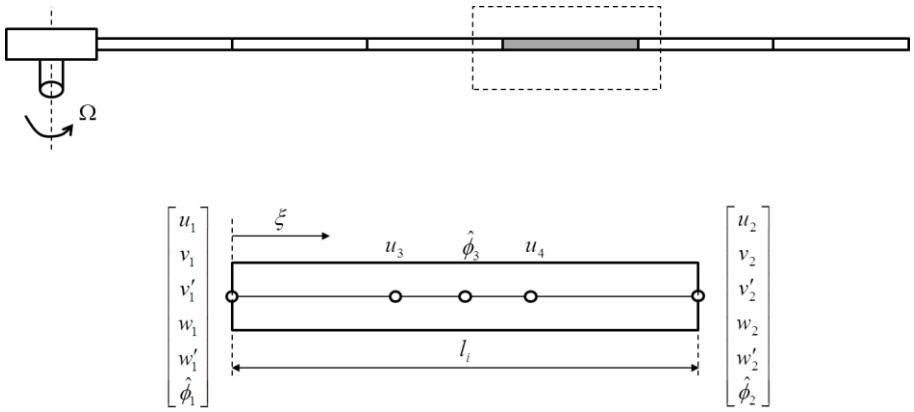

Figure 2: Sketch of the rotor blade discretized into finite elements (top); local nodes and elemental degree of freedoms (bottom)

For the *b-th* blade, neglecting the virtual work done by the aerodynamic loads, the discretized form of Eq. 1 yields

$$\delta\Pi_b = \int_0^{2\pi} \left[\sum_{i=1}^{N_{el}} \delta U_i - \delta T_i \right]_b d\Psi = 0 \tag{3}$$

with N_{el} denoting the total number of spatial finite elements and $\delta U_i - \delta T_i$ representing the virtual energy of the *i-th* blade element. Substituting Eq. 2 into Eq. 3 and assembling the elemental matrices over N_{el} spatial elements [6] gives

$$\int_0^{2\pi} \delta\mathbf{q}^T (\mathbf{M}\ddot{\mathbf{q}} + \mathbf{C}\dot{\mathbf{q}} + \mathbf{K}\mathbf{q} - \mathbf{F})\, d\Psi = 0 \tag{4}$$

where $\mathbf{q} = \mathbf{q}(\Psi)$ is the global nodal displacement vector, $\mathbf{M}, \mathbf{C} = \mathbf{C}(\Psi), \mathbf{K} = \mathbf{K}(\Psi)$ are the

global mass, damping and stiffness matrices, respectively, whereas $\mathbf{F} = \mathbf{F}(\mathbf{q}, \dot{\mathbf{q}}, \Psi)$ represents the force vector due to the structural dynamics that contains both the nonlinear terms and those independent of the elastic displacements. Then, noting that the virtual displacements, $\delta\mathbf{q}$, are arbitrary, the following final form of the blade dynamics is derived

$$\mathbf{M}\ddot{\mathbf{q}} + \mathbf{C}\dot{\mathbf{q}} + \mathbf{K}\mathbf{q} = \mathbf{F} \tag{5}$$

Equation 5 is a set of nonlinear, ordinary differential equations (ODEs) for the global elastic DOFs, forced by inertial terms; the contribution from aerodynamic loads is presented in the following subsection.

2.2 Blade Aerodynamics.

For the description of the complex aerodynamic environment that is characteristic of turbine rotor operative conditions, the modelling of unsteady, separated flow phenomena and dynamic stall effects is required. To this aim, an efficient approach is the state-space sectional formulation proposed by Beddoes-Leishman that is capable of predicting airloads in the presence of flow separation and dynamic stall onset. Within the limits of an engineering level of approximation, it provides unsteady aerodynamic loads on a translating airfoil undergoing plunge, h, and pitch, ϕ, motion in terms of nondimensional normal force *CN*, chord force *CC* and pitching moment coefficient *CM* about the sectional aerodynamic centre (see Fig. 3).

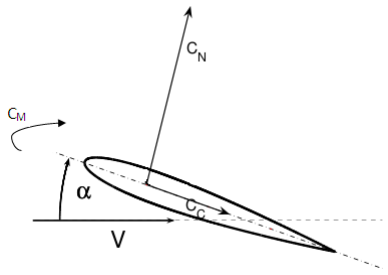

Figure 3: Definition of force and moment components

Following [8 – 10], sectional airloads are described as functions of twelve aerodynamic states $\mathbf{x} = (x_1, x_2, ..., x_{12})^T$, whose dynamics is governed by a set of ordinary differential equations. Eight states provide load terms due to attached, unsteady, compressible potential flow, three states describe nonlinear effects due to trailing-edge separation, whilst one state takes into account leading-edge flow separation effects, typical of dynamic stall occurrence. In compact form, sectional loads are given by

$$(CN, CC, CM)^T = \mathbf{f}\left(v^n_{3/4}, \alpha, \dot{\alpha}, x\right) \tag{6}$$

where $v^n_{3/4}$ is the normal component of the relative wind at the airfoil 3/4-chord point, α represents the angle between airfoil and relative wind, whereas $\mathbf{x}$ are added aerodynamic states determined as solution of the following linear ODEs

$$\dot{\mathbf{x}} = \mathbf{g}\left(\mathbf{x}, \alpha, \dot{\alpha}\right) \tag{7}$$

In details, in Eq. 7 the first two states describe the contribution of the shed-vorticity to the unsteady airloads arising in incompressible, attached flow conditions, and are related to the circulatory term of the Theodorsen theory [11]. Differently, states $(x_3, ..., x_8)$ are associated to non-circulatory loads. As the Mach number approaches zero, the $\mathbf{g}$ functions governing these states tend to become singular [12]. Thus, non-circulatory loads for incompressible flows analysis are predicted by the Theodorsen theory without inclusion of additional states [9]. Flow separation effects are modelled through the remaining four aerodynamic states of the B-L model. Three of them, namely x_9, x_{10}, x_{12}, are introduced to simulate trailing-edge separation effects: in addition to separation governed by boundary-layer dynamics, for airfoils in unsteady motion with angle of attack close to or greater than the static stall angle, they take into account also time-lag between separated-flow and fully-attached-flow force coefficients. Finally, the aerodynamic state x_{12}, represents dynamic stall effects on unsteady loads and is associated to leading-edge separation [8, 9]: this phenomenon occurs when the leading-edge pressure reaches a critical value causing the shedding of a vortex travelling over the airfoil.

The B-L model is two-dimensional. For the evaluation of rotating blades cross-section airloads, a satisfactory level of prediction accuracy is obtained by including three-dimensional rotor wake inflow effects in the evaluation of the effective downwash at the 3/4-chord point of each blade section [7]. Here, wake inflow is predicted by a Boundary Element Method (BEM) solver for attached, incompressible, potential flows [4, 5]. In details, the perturbation velocity induced by the rotor wake is evaluated at the rear neutral point of each section and is used to modify/enhance the downwash forcing the ODEs governing the aerodynamic states x_1 and x_2 in Eqs. 6 and 7. The proposed methodology provides good predictions of rotor airloads within the assumption of light stall. At high angles of attack, deep stall and post-stall regimes are characterized by massive flow separation. In the framework of wind turbines aeroelastic analyses for preliminary design, semi-empirical corrections are typically introduced to provide realistic overall performance predictions at reduced computational costs. Thus, the Viterna-Corrigan approach, based on a flat plate theory approximation [13], is herein used to extend static aerodynamic coefficients to high angle-of-attack operation range, where experimental lift and drag airfoil characteristics are not easily available [14]. Moreover, due to the centrifugal pumping effect, stall regime for rotating blades starts at higher angles of attack with respect to airfoils statically tested in wind tunnels [14]. A widely used empirical description of this effect, based on the laminar boundary layer theory, is presented in [15].

From the above considerations the external virtual work, δW_b, done by the aerodynamic loads acting upon the *b-th* blade is defined. To this aim, firstly $\alpha, \dot{\alpha}$ and $v^n_{3/4}$ are evaluated at the blade cross sections, accounting for wind velocity, blade motion and deformation and wake inflow. Thus, since $\alpha, \dot{\alpha}$ and $v^n_{3/4}$ depend of blade elastic displacements, the sectional loads given by Eqs.(6)-(7) are nonlinear functions of the blade elastic states, making the determination of the generalized aerodynamic loads inherently coupled with blade structural dynamics. Then, denoting with $\Re(x'y'z')$ the local deformed blade frame of reference and

with $\Re(xyz)$ the undeformed blade frame of reference centred at rotor hub and rigidly connected to the blade (see Fig. 1), the sectional loads are expressed in the undeformed blade frame of reference through a rotational matrix, $\mathbf{T}$, depending of the elastic displacement field [2]. The vector of sectional dimensional airloads may be then written as $\mathbf{L}_{\mathbf{A}}^{\mathbf{T}} = \left[L_u, L_v, L_{w,} M_\phi \right]$. Further, for $\delta \mathbf{u}^T = \left[\delta u, \delta v, \delta w, \delta \phi \right]$ denoting the virtual elastic displacement, the virtual work done by the aerodynamic loads on the *b-th* blade is

$$\delta W_b = \int_0^R \delta \mathbf{u}^T \mathbf{L}_A \, dx \tag{8}$$

with R representing blade radius. By applying the FEM discretization, Eq. 8 is recast in the following form

$$\delta W_b = \sum_{i=1}^{N_{el}} \delta \mathbf{q}_i^T \int_0^{L_i} \mathbf{H}^T \mathbf{L}_{\mathbf{A}_i} \, d\xi \tag{9}$$

where L_i denotes the length of the *i-th* finite element and $\mathbf{L}_{\mathbf{A_i}}$ is the vector of sectional loads evaluated within the *i-th* finite element. It is worthy note that, since $\mathbf{T} = \mathbf{T}(\mathbf{q})$, $\alpha = \alpha(\mathbf{q}, \dot{\mathbf{q}}, \Psi)$, $\dot{\alpha} = \dot{\alpha}(\dot{\mathbf{q}}, \ddot{\mathbf{q}}, \Psi)$ and $v_{3/4}^n = v_{3/4}^n(\mathbf{q}, \dot{\mathbf{q}}, \ddot{\mathbf{q}}, \Psi)$, $\mathbf{L}_{\mathbf{A}i} = \mathbf{L}_{\mathbf{A}i}(\mathbf{q}, \dot{\mathbf{q}}, \ddot{\mathbf{q}}, \Psi)$ is a nonlinear function of the global DOF's.

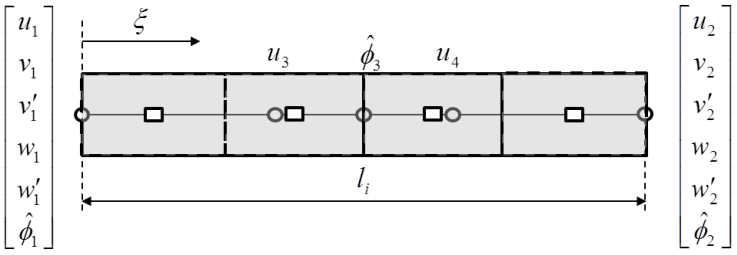

Figure 4: Finite element nodes (circles) and aerodynamic stations (squares)

Finally, dividing the *i-th* finite element into N_{ae} aerodynamic segments of length $\Delta\xi$ centred at ξ_k (see Fig. 4), Eq. 9 becomes

$$\delta W_b = \sum_{i=1}^{N_{el}} \delta \mathbf{q}_i^T \sum_{k=1}^{N_{ae}} [\mathbf{H}^T \mathbf{L}_{A_i}]_k \Delta\xi \tag{10}$$

in which $\left[\bullet \right]_k$ indicates aerodynamic force contributions evaluated at ξ_k. By combining Eq. 10 with Eq. 3 and assembling over the N_{el} elements, the aerodynamic vector load $\mathbf{F}_A = \mathbf{F}_A(\mathbf{q}, \dot{\mathbf{q}}, \ddot{\mathbf{q}}, \Psi)$ is given by

$$\mathbf{F}_A = \sum_{k=1}^{N_{ae}} [\mathbf{H}^T \mathbf{L}_{A_i}]_k \Delta\xi \tag{11}$$

thus yielding the following form of the aeroelastic equations for the *b-th* blade

$$\mathbf{M}\ddot{\mathbf{q}} + \mathbf{C}\dot{\mathbf{q}} + \mathbf{K}\mathbf{q} = \mathbf{F} + \mathbf{F}_A \tag{12}$$

which are then solved through a Crank-Nicolson time-marching scheme.

3 NUMERICAL RESULTS AND DISCUSSION

The proposed FEM aeroelastic tool is herein validated through comparison with available analytical, numerical and experimental data. Applications firstly concern structural and aeroelastic analyses of helicopter rotors in hovering.

A nonrotating Bernoulli-type linear beam clamped at root and undergoing uncoupled elastic twist, flap and lag deformation is considered first. Beam structural and geometric properties are summarized in Table 1 (left). Beam eigenfrequencies are presented in Table 1 (right) showing good correlation of present FEM predictions with analytical results. The same level of accuracy of numerical results is shown in Table 2 for the two-bladed hingeless rotor experimentally tested in [16]. The comparison is performed for a torsionally soft rotor with zero precone, droop and collective pitch, considering both a soft and a stiff flexure.

Table 1: Non-rotating beam: geometric and structural properties (left), predicted eigenfrequencies compared to analytical results (right)

Geometric & Structural properties	
Length [m]	5.029
Lag bending stiffness [Nm^2]	$8 \cdot 10^5$
Flap bending stiffness [Nm^2]	$6 \cdot 10^5$
Torsion stiffness [Nm^2]	$1 \cdot 10^6$

Beam eigenfrequencies [rad/s]		
	Analytical	FEM
I lag	87.91	87.92
II lag	551.01	551.02
III lag	1542.97	1542.96
I flap	32.10	32.10
II flap	201.19	201.20
III flap	563.41	563.40
I torsion	321.56	321.56
II torsion	964.69	964.69
III torsion	1607.82	1607.90

Table 2: Two-bladed hingeless rotor: FEM predictions compared to experimental data in [16]

Non-rotating blade natural frequencies [Hz]				
	Soft Flexure		Stiff Flexure	
	EXP	FEM	EXP	FEM
I lag	22.02	22.56	23.76	23.34
I flap	5.19	5.18	5.25	5.19
II flap	32.50	32.69	32.75	32.8
I torsion	38.38	36.5	44.73	43.59

Table 3: Four-bladed hingeless rotor: present predictions compared to data in [17]

Rotating blade natural frequencies [Hz]		
	FEM [17]	Present FEM model
I lag	4.71	4.63
II lag	27.95	28.0
III lag	70.67	70.44
I flap	7.38	7.42
II flap	21.71	21.59
III flap	47.98	47.78
I torsion	22.69	22.51
II torsion	10.445	10.428

Then, rotating frequencies and natural mode shapes of a four-bladed hingeless helicopter rotor in hovering are addressed. Vehicle properties are described in [17]: rotor blades are uniform with a linear pre-twist of -8°. A collective pitch angle of 9° is used to couple blade flap, lag and torsion modes. Blades natural frequencies predicted by the present FEM model are listed in Table 3 showing a good level of accuracy with respect to results from the FEM approach proposed in [17]. The same high quality of numerical prediction is achieved for the first three flap and lag bending modes as well as for the first two torsion modes (see Fig. 5).

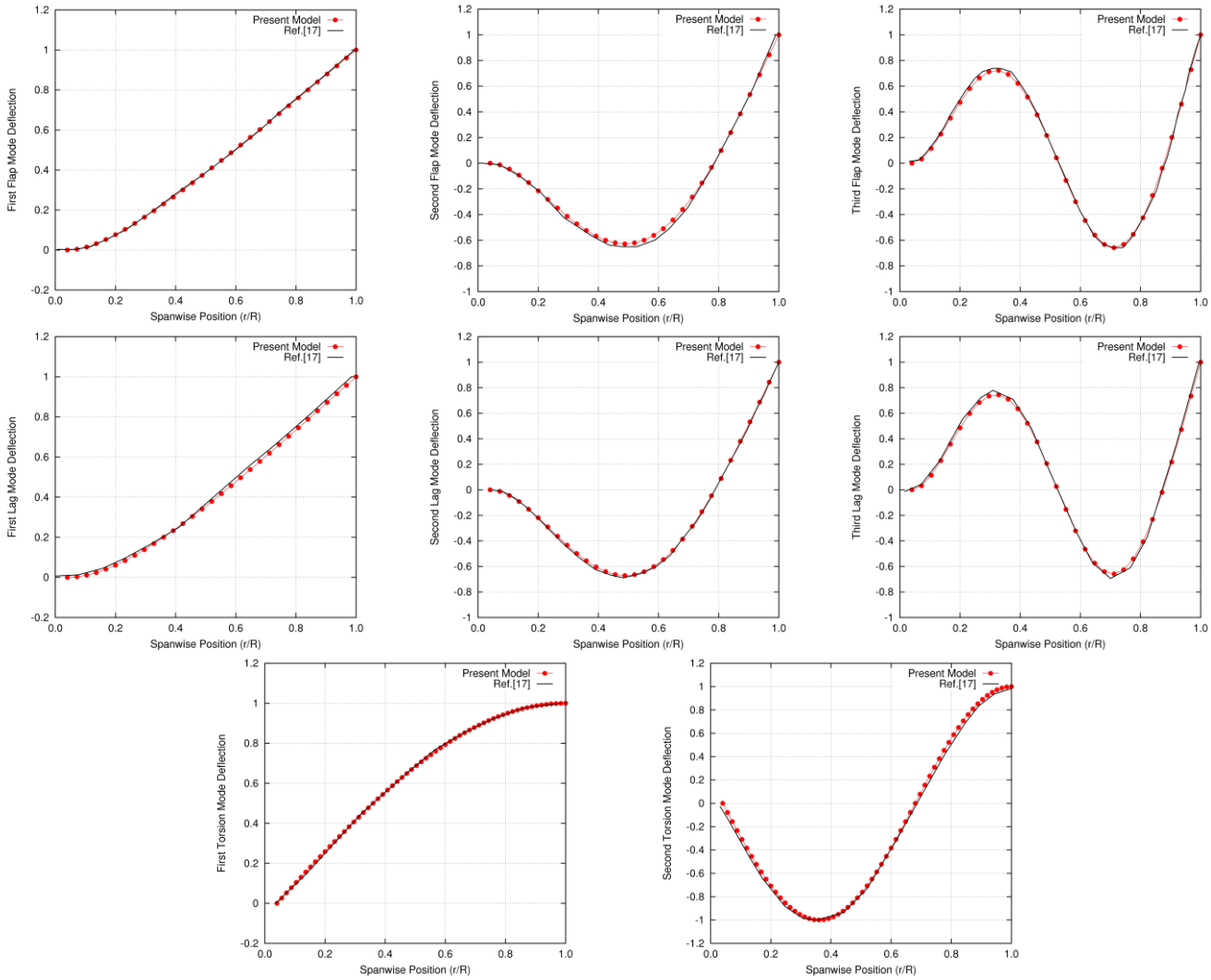

Figure 5: FEM predictions of blade natural modes shapes for a four-bladed hingeless helicopter rotor: present approach compared to data in [17]

The present FEM numerical tool is then applied to the aeroelastic analysis of a two-bladed hingeless helicopter rotor in hover. Detailed description of the test case can be found in [18]: rotor blades are untwisted, without structural damping, root offset and chordwise axis offset. The blade has NACA 0012 airfoil sections and a rectangular planform shape, and the rotor is operating at an angular velocity of 1000 rpm. Structural properties of the blade are found in

[18]. Several values of collective pitch θ are considered along with two precone settings ($\beta = 0°$ and $\beta = 5°$). First, the proposed blade aerodynamics model is validated assuming a rigid bladed rotor. Figure 6 shows predicted thrust loading along blade span for $\theta = 8°$ and $\beta = 0°$. Nondimensional loading coefficient is herein defined as $dc_T/ds = (2\,dT/dr)/\rho V^2 c$, where $s = r/R$, dT denotes section elemental thrust, ρ is the air density, V is the local total velocity and c the section chord. For the present assessment B-L aerodynamics model is enhanced by the rotor wake inflow provided by a 3D BEM solver to correct blade sections downwash. This approach can suitably enhance B-L sectional aerodynamics with respect to a simple momentum theory approach yielding numerical predictions that are in excellent agreement with BEM outcomes up to 80% of blade span. Nevertheless, the inclusion of rotor wake inflow is not sufficient to correctly predict airloads near blade tip (see [7]).

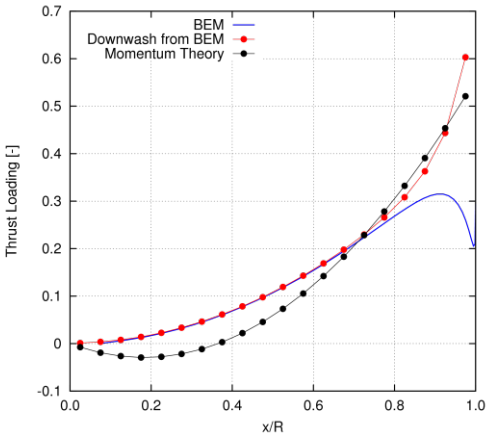

Figure 6: Thrust loading along span for a rigid blade ($\theta = 8°$ and $\beta = 0°$)

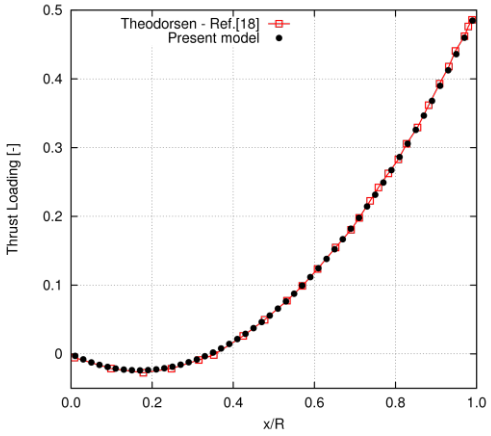

Figure 7: Thrust loading along blade span for a deformable blade ($\theta = 8°$ and $\beta = 0°$)

For the same rotor, blade deformations are then addressed. The present formulation is compared to the modal approach proposed in [18] where the Theodorsen theory [11] is used to describe blade sections airloads. The FEM analysis is herein performed using 50 elements along blade span to ensures negligible sensitivity to further refinements. In order to validate the proposed aeroelastic tool, for the present steady calculation, only states x_1 and x_2 of B-L aerodynamics, which are associated to the circulatory terms derived in the Theodorsen theory (see [11, 12]), are activated, whilst BEM wake inflow is not included. This yields an excellent agreement with numerical results in [18] in terms of thrust loading acting on a deformable blade (see Fig. 7). The same quality of predictions is achieved for blade tip flap, lag and torsion displacements at several collective pitch settings and for $\beta = 0°$ and $\beta = 5°$, as shown in Fig. 8.

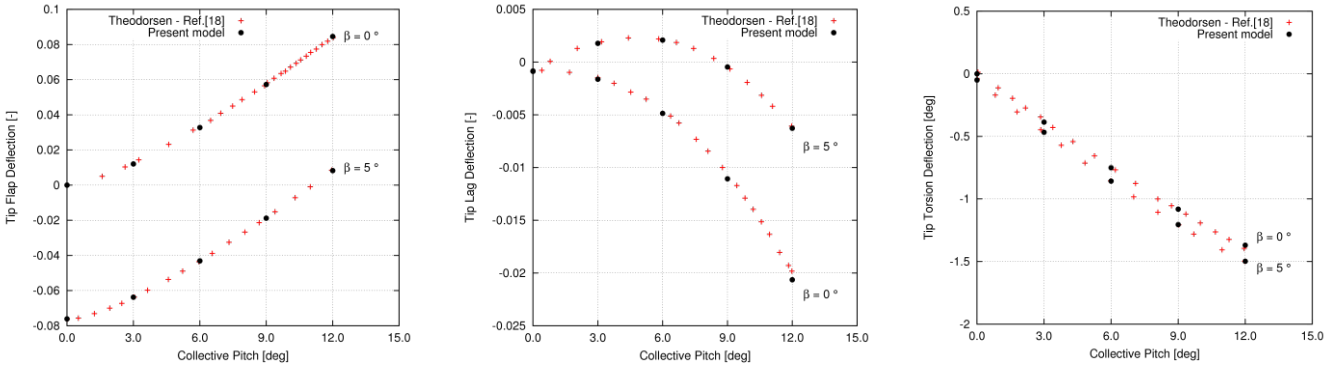

Figure 8: Predicted blade tip displacements for a two-bladed hingeless helicopter rotor in hover: present approach compared to data in [18]

Next, the aeroelastic analysis of the NREL Phase VI wind turbine [19] is presented. It is a 10.58 m diameter, two-bladed rotor with cross-sections having the shape of S809 airfoils starting from radial position at 1/4 of the blade, and circular shape at the root region (transition from circular to non-circular sections is achieved through a conical surface, as shown in Fig. 9). In the 3/4-radius outer region, the blades are linearly tapered, with a non-linear distribution of twist (see Fig. 9). Further details on rotor mechanical and geometrical characteristics can be found in [19, 20]. The following numerical simulations have been obtained considering a constant blade pitch of 3° at the tip section, and null precone angle.

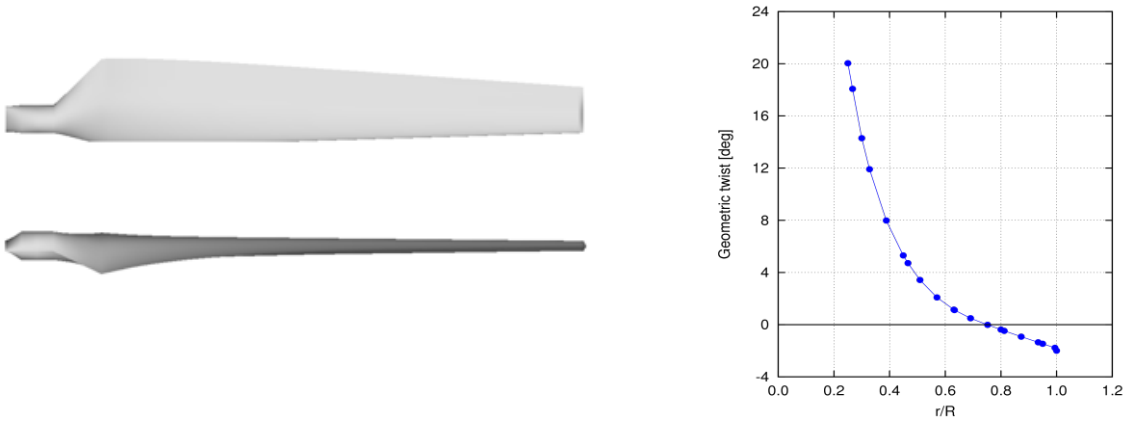

Figure 9: CAD rendering of NREL wind turbine blade (left) and distribution of the geometric twist along the blade (right)

The distribution of blade stiffness characteristics provided in [19] yields very small blade deflections. This is proven in Fig. 10, where blade tip bending displacements evaluated for wind speed $5\,m/s \le V_W \le 10\,m/s$ are depicted. In the same speed range, predicted blade tip torsion (not shown) is almost zero. Present results are compared to those provided by a validated aeroelastic solver based on the Galërkin modal approach applied to the same structural and aerodynamic model used herein [7].

Finally, the proposed aeroelastic tool is applied to predict wind turbine delivered power at the steady equilibrium condition. A crucial issue related to the use of the BEM solver to adapt

airfoil theories to wind turbine aerodynamics applications is the definition of the range of section angle of attack and wind speed in which it can be conveniently used without incurring in non-physical high values of induced velocity. For the present preliminary results, the numerical analysis is limited to a wind speed range yielding attached flow conditions along the blade. The accuracy of wind turbine power predictions is examined in Fig. 11, which shows that the present approach is in good agreement with measurements in the range $5\,m/s \le V_W \le 9\,m/s$. In order to improve global loads predictions at high-angle-of-attack conditions, *i.e.* $V_W \ge 10\,m/s$, flat-plate formulas modified with Snel centrifugal pumping correction should be included in the model. Guidelines to face this issues are proposed in [7] following the CFD simulations in [21, 22] and will be implemented in further developments of the present work.

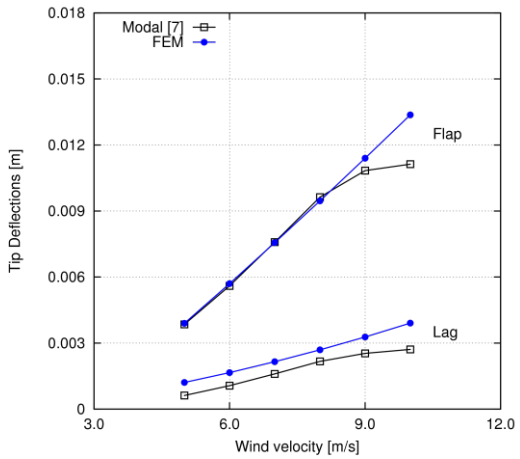

Figure 10: Turbine flap and lag bending blade tip displacements

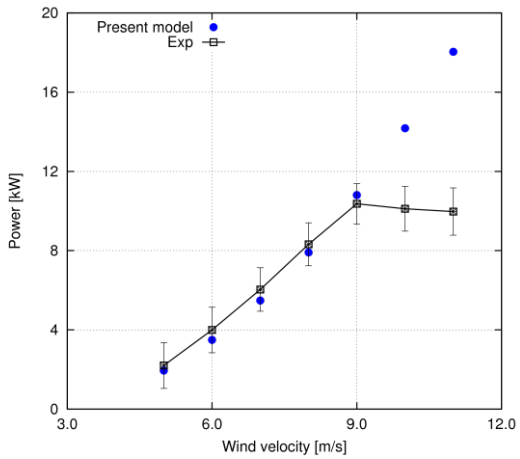

Figure 11: Turbine power predictions

4 CONCLUSIONS

An aeroelastic formulation based on the Finite Element Method for performance and stability predictions of isolated horizontal axis wind turbines has been developed. A general formulation that might be extended to include the presence of the tower and floating structures for off-shore applications as well as to face the analysis of advanced-shape blades, is proposed. It represents the starting point of an ongoing research activity on wind energy aimed at the development of a comprehensive aeroelastic code for wind turbines analysis. As a consequence, results have to be considered as preliminary. Hamilton's principle is used to derive a nonlinear formulation to model the structural dynamics of non-uniform rotor blades described as long, straight, slender, homogeneous isotropic beams undergoing axial, lag, flap and torsion displacements. A devoted fifteen-degrees-of-freedom finite element to accurately model kinematics and elastic behavior of rotating blades is introduced. Blade aerodynamics is simulated by the unsteady sectional Beddoes-Leishman state-space formulation to include effects of nonlinear phenomena, such as static and dynamic stall, whilst wake inflow effects are modelled either by the simple momentum theory approach, or by a more advanced

unsteady, three-dimensional, free-wake Boundary Element Method. Discretization of the aeroelastic equations is then carried-out to yield a set of coupled nonlinear ordinary differential equations solved by a time-marching algorithm. Due to the similarities between helicopter and wind-turbine rotor blades, for validation purposes different types of helicopter main rotors in hovering have been considered. Blade non-rotating and rotating natural frequencies and modes shapes, as well as section airloads and steady-state aeroelastic tip flap, lag and torsion displacements are predicted with very good agreement with respect to numerical and experimental literature data. Next, considering a horizontal axis wind turbine model in an homogeneous onset-flow, blade response and delivered power are predicted. Comparison with experimental data and with a well-assessed and validated aeroelastic modal approach based on the same structural and aerodynamic model used herein shows a good capability of the present formulation to predict blade deformations and rotor delivered power up to the onset of stall. Further developments of the present work include the application of the widely-used Viterna-Corrigan formulas, modified through Snel centrifugal pumping correction to extend to massively separated flow (high wind speed) conditions the accurate prediction of wind turbine performance.

AKNOWLEDGEMENTS

This work has been partially supported by the Flagship Project "RITmare, Italian Research for the sea" founded by the Italian Ministry of University and Research (MIUR).

REFERENCES

[1] Zhang, P. and Huang, S. *Review of Aeroelasticity for Wind Turbine: Current Status, Research Focus and Future Perspectives. Frontiers in Energy*. Vol.5 (2011) **4**:419-434.

[2] Hodges, D.H. and Dowell, E.H. *Nonlinear Equations of Motion for the Elastic Bending and Torsion of Twisted Nonuniform Rotor Blades*. NASA TN D-7818 (1974).

[3] Hodges, D.H. and Ormiston, R. *Stability of Elastic Bending and Torsion of Uniform Cantilever Rotor Blades in Hover with Variable Structural Coupling*. NASA TND8192 (1976).

[4] Greco, L., Muscari, R., Testa, C. and Di Mascio, A. Marine Propellers Performance and Flow-Field Features Prediction by a Free-Wake Panel Method. *Journal of Hydrodynamics* Ser.B Vol.6 (2014) **5**:780-795.

[5] Gennaretti, M. and Bernardini, G. Novel Boundary Integral Formulation for Blade-Vortex Interaction Aerodynamics of Helicopter Rotors. *AIAA Journal* Vol.45 (2007) **6**:175-184.

[6] Shrinivas, R.B. and Ranjan, G. Validation of Comprehensive Helicopter Aeroelastic Analysis with Experimental data. *Defence Science Journal* Vol.54 (2004) **4**:419-427.

[7] Calabretta, A., Molica Colella, M., Greco, L. and Gennaretti, M. Assessment of Aerodynamics Models for Wind Turbines Aeroelasticity. *Proceedings of the Conference on Advances in Civil, Environmental and Materials Research (ACEM2014)*. Busan, South Korea (2014).

[8] Leishman, J.G. and Crouse, G.L.Jr. State-Space Model for Unsteady Airfoil Behavior and Dynamic Stall. *AIAA Paper* 89-1319 (1989) 1372-1383.

[9] Hansen, M.H., Gaunaa, M. and Madsen, H.A. *A Beddoes-Leishman Type Dynamic Stall Model in State Space and Indicial Formulation*. Risoe Technical Report No.1354(EN) (2004).
[10] Leishman, J.G. and Beddoes, T.S. A Semi-Empirical Model for Dynamic Stall. *Journal of American Helicopter Society* Vol.34 (1989) **3**:3-17.
[11] Theodorsen, T. *General Theory of Aerodynamic Instability and the Mechanism of Flutter*. NACA Report 496 (1935).
[12] Calabretta, A., Molica Colella, M., Greco, L., Dubbioso, G., Testa, C. and Gennaretti, M. A Comprehensive Numerical Model for Horizontal Axis Wind Turbines Aeroelasticity. *Proceedings of the Conference on Wind Energy Science and Technology (RUZGEM2013)*. Ankara, Turkey (2013).
[13] Shepers, J.G., Brand, A.J., Bruining, A., Graham, J.M.R., Hand, M.M., Infield, D.G., Madsen, H.A., Paynter, J.H., van Rooji, R., Shimizu, Y. and Simms, D.A. *Final Report of IEA Annex XIV: field rotor aerodynamics*. ECN-C-97-027, Netherlands Energy Research Foundation (1997).
[14] Martinez, J., Bernabini, L., Probst, O. and Rodriguez, C. An Improved BEM model for the Power Curve Prediction of Stall-regulated Wind Turbines. *Wind Energy* Vol.8 (2005) 385-402.
[15] Snel, H., Houwink, R., Bosschers, J., Piers, W.J., van Bussel, G.J.W. and Bruining, A. Sectional Prediction of 3-D Effects for Stalled Flow on Rotating Blades and Comparison with Measurements. *Proceedings of the European Community Wind Energy Conference*, Lübeck-Travemünde, Germany (1993).
[16] Sharpe, D.L. A Comparison of Theory and Experiment for Aeroelastic Stability of a Hingeless Rotor Model in Hover. *Proceedings of the Integrated Technology Rotor Methodology Assessment Workshop*, Moffett Field (CA, USA) (1983).
[17] Zhang, J. *Active-passive Hybrid Optimization of Rotor Blades with Trailing Edge Flaps*. The Pennsylvania State University, PhD Thesis (2001).
[18] Kwoon, O.J. *A technique for the prediction of aerodynamics and aeroelasticity of rotor blades*. Georgia Institute of Technology, PhD Thesis (1988).
[19] Hand, M.M., Simms, D.A., Fingersh, L.J., Jager, D.W., Cotrell, J.R., Schreck, S. and Larwood, S.M. *Unsteady Aerodynamics Experiment Phase VI: Wind Tunnel Test Configuration and Available Data Campaigns*. NREL/TP-500-29955 (2001).
[20] Gigure, P. and Selig, M.S. *Design of a Tapered and Twisted Blade for the NREL Combined Experiment Rotor*. NREL/SR-500-26173 (1999).
[21] Yelmule, M.M. and Anjuri, E.VSJ. CFD Predictions of NREL Phase VI Rotor Experiments in NASA/AMES Wind Tunnel. *International Journal of Renewable Energy Research* Vol.3 (2013) **2**:261-269.
[22] Sorensen, N.N., Michelsen, J.A. and Schreck, S. Navier-Stokes Predictions of the NREL Phase VI Rotor in the NASA Ames 80ft x 120ft Wind Tunnel. *Wind Energy* Vol.5 (2002) 151-169.